# The boundary layer near the stagnation point in hypersonic flow past a sphere

By T. K. HERRING
Department of Mathematics, University of Manchester

(Received 13 May 1959)

When a sphere or other bluff body travels at supersonic speeds, a shock wave is formed close to the front surface. With increase of speed the air behind the shock is further compressed, and the shock wave moves closer to the surface. This paper considers the case where the region close to the stagnation point between the shock and the sphere can be taken to be a steady laminar boundary layer.

The approximate solution of the equations of motion follows closely the classical work of Homann (1936), ideas similar to those of Lighthill (1957) being used to apply it to the problem in hand. It consists mainly in reducing the equations to ordinary differential form by assuming forms of the flow variables which satisfy the boundary conditions, notably at the shock wave. In addition, several transformations are employed in order to simplify the equations and to increase the range of solutions, and also to facilitate the use of the 'Mercury' electronic computer in solving them.

The results give an insight into some aspects of hypersonic flows. Included in this paper are a selection of temperature and transverse velocity profiles across the boundary layer and several graphs relating such quantities as the shock stand-off distance and the skin-friction coefficient with Reynolds number. The last two mentioned are the most interesting. The first set gives the surprising result that the shock stand-off distance increases with increase in Reynolds number, whereas it is known that the boundary-layer thickness decreases. The second set of graphs shows that the skin-friction coefficient is inversely proportional to a decreasing power of the Reynolds number when it is lower than order $10^3$, but the indication is that it tends to the expected constant power of $\frac{1}{2}$ when the Reynolds number is of order $10^4$.

## 1. Introduction

In this paper we investigate an interesting case where the region between the shock and the sphere can be taken to be a steady laminar boundary layer. A high-speed flow through a medium of very low density would seem to satisfy this condition. For, at low enough density, the Reynolds number can be so low (say, about $10^4$ or less) that the boundary layer will be laminar, but of a thickness comparable to the stand-off distance of the shock.

Now, in the atmosphere at heights of 60–100 km, the densities range from $10^{-6}$ to $10^{-7.5}$ g/cm$^3$, and the temperatures vary from 180° to 360° K (Whipple 1943). The Reynolds number of a sphere of diameter 25 cm, travelling at 4 km/sec

at an altitude of 80 km, is about $5 \times 10^3$. This region of the atmosphere thus provides a practical setting for the problem under investigation.

We shall assume that the surface of the body has not yet been heated significantly, and thus that it is a good approximation to take the sphere and free stream temperatures to be equal.

By confining ourselves to the region close to the stagnation point, the shock wave can be taken, to a fair approximation, as spherical and concentric with the sphere. This is a result which has been verified under certain conditions both experimentally and theoretically. Oliver (1956) showed in experiments with a sphere and other bluff bodies at a Mach number of 5·8 that this was so, and he included in his paper excellent schlieren photographs of the phenomenon. A number of authors, including Lighthill (1957), Freeman (1956) and Chester (1956), have put forward theoretical treatments. Chester considered a perfect gas with constant specific heats (as we shall), and, by a method of successive approximations in which he assumed the shape of the shock and found the shape of the body, he was able to verify the above results.

Now, close to the stagnation point the speeds are subsonic, and all compressibility effects are due to thermal variations in the fluid properties. The present work can therefore be compared with work on low-speed laminar boundary layers with varying temperatures. For example, Brown & Donoughe (1951) considered the problem of a two-dimensional steady laminar boundary layer on a straight porous wall, and they found solutions to the equations of motion when the wall temperature was varied. They were able to obtain a negative displacement thickness by cooling the wall, a result similar to one in this paper where the stand-off distance of the shock is found to increase with Reynolds number.

The geometry of the problem we are considering is close to that of Homann (1936), who considered the steady incompressible flow in a boundary layer, along a surface of revolution, close to the stagnation point. He neglected terms of the order of the square of the transverse co-ordinate measured along the surface, and found that the form of the flow variables suggested by the axial symmetry and the constant thickness of the boundary layer, which is a correct result in this approximation, satisfied the boundary conditions and the equations of motion.

In the paper by Lighthill (1957), an exact solution to the inviscid incompressible high-speed flow past a sphere was obtained. Lighthill showed that all the equations of motion and boundary conditions could be satisfied assuming a spherical shock concentric with the sphere.

For the present problem we combine the approaches of Homann and Lighthill, using the forms of the flow variables suggested by the boundary conditions behind the shock wave. The use of the strong-shock conditions is found to be necessary to make the density dependent upon the normal co-ordinate yet independent of the transverse co-ordinate to the first order. With this simplification, the assumed forms of the flow variables satisfy the boundary conditions accurately. The inviscid terms of the equations of motion are satisfied accurately, and the viscous terms are satisfied to the first order in the transverse co-ordinate. A note on the approximation involved in using the strong-shock relations is included in §3.

We will assume for simplicity that the fluid is a perfect gas and that the specific heats at constant pressure and volume of the gas mixture are constant throughout the region of interest. In a real flow, however, where there are very large temperature differences in the boundary layer, the variations in the ratio of the specific heats can be as much as 0·3. This is attributable to ionization and dissociation effects as well as to the large range of temperatures. For this reason we shall quote results for different ratios of the specific heats.

The first section of the paper is devoted to the formulation and simplification of the equations of motion, and several transformations are introduced to facilitate subsequent integrations. The second section concerns the derivation of the results and the discussion of interesting physical conclusions.

## 2. Basic equations

The equation of state of a perfect gas is

$$p = \rho RT, \tag{1}$$

where $R$ is the gas constant per gramme, $p$ the pressure, $\rho$ the density, and $T$ the temperature. To simplify the problem further, we will take the viscosity $\mu$ to be proportional to $T$, and the Prandtl number $\sigma = \mu c_p/k$ to be a constant = 0·72. Here $c_p$ and $c_v$ are the specific heats at constant pressure and volume ($c_p/c_v = \gamma$), and $k$ is the thermal conductivity, which must also be proportional to $T$.

We shall use spherical polar co-ordinates $(r, \theta, \lambda)$ with origin at the centre of the sphere and the axis $\theta = 0$ pointing upstream, and write the respective velocity components as $v_r, v_\theta, v_\lambda$, with $v_\lambda = 0$ in the present case of axial symmetry. The radius of the sphere is taken to be $a$, and that of the shock to be $b$, and suffixes 0, 1 will refer respectively to the uniform conditions ahead of the shock, and those immediately behind. Also, we will denote the enthalpy by $I$ and let $M_0 = V_0/c_0$, $c_0$, and $V_0$ be the values of the Mach number, speed of sound and axial velocity ahead of the shock. It is important to note that throughout this paper we are considering only the region where $\theta$ is small (shaded in figure 1).

The strong-shock relations are

$$\frac{\rho_1}{\rho_0} = \frac{\gamma+1}{\gamma-1}, \tag{2}$$

$$v_{r1} = -\frac{\gamma-1}{\gamma+1} V_0 \cos\theta, \quad v_{\theta 1} = V_0 \sin\theta, \tag{3}$$

$$\frac{p_1}{p_0} = \frac{2\gamma}{\gamma+1} M_0^2 \cos^2\theta, \tag{4}$$

and

$$\frac{I_1}{I_0} = \frac{T_1}{T_0} = \frac{\mu_1}{\mu_0} = \frac{2\gamma(\gamma-1) M_0^2}{(\gamma+1)^2}. \tag{5}$$

These shock boundary conditions suggest that it may be useful to investigate whether an approximate solution with

$$v_r = v(r)\cos\theta, \quad v_\theta = u(r)\sin\theta, \tag{6}$$

$$\rho = \rho(r), \quad p = p(r) + P(r)\sin^2\theta, \tag{7}$$

may exist. The more complicated form of $p$ is particularly suited to a boundary-layer type of theory, which is well known to be sensitive to the effect of pressure gradient. The assumptions (6) and (7) correspond to those of Homann (1936) and Lighthill (1957).

The equations of motion in spherical polar co-ordinates are reduced to the axisymmetric boundary-layer form by dimensional considerations and are listed below. The continuity equation becomes

$$\frac{\partial}{\partial r}(\rho v_r)+\frac{1}{a\sin\theta}\frac{\partial}{\partial\theta}(\sin\theta\rho v_\theta)=0, \tag{8}$$

and the momentum equation for the $\theta$-direction becomes

$$\rho\left(v_r\frac{\partial v_\theta}{\partial r}+\frac{v_\theta}{a}\frac{\partial v_\theta}{\partial\theta}\right)=-\frac{1}{a}\frac{\partial p}{\partial\theta}+\frac{\partial}{\partial r}\left(\mu\frac{\partial v_\theta}{\partial r}\right), \tag{9}$$

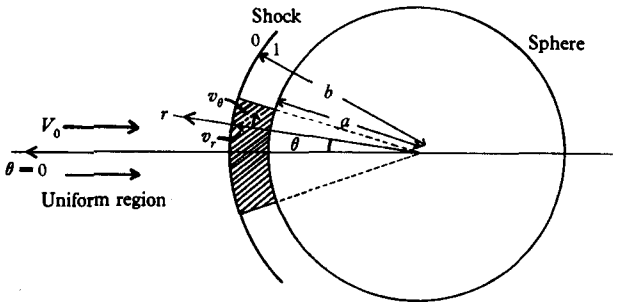


FIGURE 1

whilst the energy equation reduces to

$$\rho\left(v_r\frac{\partial I}{\partial r}+\frac{v_\theta}{a}\frac{\partial I}{\partial\theta}\right)-\frac{v_\theta}{a}\frac{\partial p}{\partial\theta}=\frac{1}{\sigma}\frac{\partial}{\partial r}\left(\mu\frac{\partial I}{\partial r}\right)+\mu\left(\frac{\partial v_\theta}{\partial r}\right)^2, \tag{10}$$

where

$$I=c_pT. \tag{11}$$

In accordance with the usual boundary-layer theory, the pressure gradient across the layer is neglected, so that, in (9), $\partial p/\partial\theta$ is found from its value immediately behind the shock, which is assumed to be within the boundary layer. Thus (4) gives

$$\frac{\partial p_1}{\partial\theta}=-\frac{4\gamma}{(\gamma+1)}M_0^2\sin\theta\cos\theta p_0;$$

and by replacing $M_0^2$ by $V_0^2/c_0^2$ and then $c_0^2$ by $\gamma p_0/\rho_0$, this becomes

$$\frac{\partial p_1}{\partial\theta}=-\frac{4(\gamma-1)}{(\gamma+1)^2}V_0^2\rho_1\sin\theta. \tag{12}$$

On substituting for $\partial p/\partial\theta=\partial p_1/\partial\theta$ in (9), we get

$$\rho\left(v_r\frac{\partial v_\theta}{\partial r}+\frac{v_\theta}{a}\frac{\partial v_\theta}{\partial\theta}\right)=\frac{4(\gamma-1)}{(\gamma+1)^2}\frac{V_0^2}{a}\rho_1\sin\theta+\frac{\partial}{\partial r}\left(\mu\frac{\partial v_\theta}{\partial r}\right). \tag{13}$$

To compare this work with that of Homann, expressed in the boundary-layer co-ordinates $(x,y)$, we simply replace $a\theta$ and $a\sin\theta$ by $x$, and $r-a$ by $y$. On

substituting for the flow variables the forms (6) and (7), we are able to reduce the equations of motion to ordinary differential form. Equation (13) becomes

$$\left[\rho\left(v\frac{du}{dr}+\frac{u^2}{a}\right)-\frac{4(\gamma-1)\,V_0^2\rho_1}{(\gamma+1)^2\,a}-\frac{d}{dr}\left(\mu\frac{du}{dr}\right)\right]\sin\theta=0; \tag{14}$$

and we shall also use (10) for $\theta = 0$, namely

$$\rho v\frac{dI}{dr}-\frac{1}{\sigma}\frac{d}{dr}\left(\mu\frac{dI}{dr}\right)=0, \tag{15}$$

where henceforth $I(r)$, $T(r)$, $\mu(r)$ will signify values for $\theta = 0$.

To satisfy the continuity equation, we now choose a Stokes stream function $\psi$, such that

$$a\sin\theta\rho v_r=-\rho_1\frac{\partial\psi}{\partial\theta}\quad\text{and}\quad\sin\theta\rho v_\theta=\rho_1\frac{\partial\psi}{\partial r}; \tag{16}$$

and on substituting (6), we see that $\psi$ takes the form

$$\psi=\Psi(r)\sin^2\theta, \tag{17}$$

and (16) reduces to

$$v=-\frac{2}{a}\frac{\rho_1}{\rho}\Psi\quad\text{and}\quad u=\frac{\rho_1}{\rho}\frac{d\Psi}{dr}. \tag{18}$$

*Transformation of the equations*

The effect of compressibility is made less marked by choosing a Howarth variable

$$\eta=C\int_a^r\frac{\rho(\beta)}{\rho_1}d\beta, \tag{19}$$

$C$ being a constant. We put also

$$\Psi(r)=Bf(\eta), \tag{20}$$

where $B$ is another constant, and

$$g(\eta)=\frac{I(r)}{I_1}=\frac{T(r)}{T_1}=\frac{\rho_1}{\rho(r)}. \tag{21}$$

Equations (18) now become

$$v(r)=-\frac{2}{a}\frac{\rho}{\rho(\eta)}Bf(\eta),\quad u(r)=BCf'(\eta), \tag{22}$$

where the prime signifies differentiation with respect to $\eta$; and substituting (22) in equation (14), we get

$$-2\frac{B^2C^2}{a}ff''+\frac{B^2C^2}{a}f'^2-\frac{4(\gamma-1)}{(\gamma+1)^2}\frac{V_0^2}{a}g-\frac{d}{d\eta}\left(\frac{\mu\rho}{\mu_1\rho_1}f''\right)BC^3\nu_1=0.$$

Now, since $\mu\rho = \text{const.}$, if we choose

$$C=\left(\frac{V_0}{\nu_1 a}\right)^{\frac{1}{2}}\quad\text{and}\quad B=(V_0\nu_1 a)^{\frac{1}{2}}, \tag{23}$$

the above equation reduces to

$$f'''+2ff''-f'^2+\frac{4(\gamma-1)}{(\gamma+1)^2}g=0, \tag{24}$$

and the energy equation (18) becomes

$$g''+2\sigma fg'=0, \tag{25}$$

where the Prandtl number $\sigma = 0{\cdot}72$ for air.

The equations (24) and (25) represent a fifth-order system, but in addition the stand-off distance of the shock is unknown. We require therefore six boundary conditions to solve the equations. These are listed below.

First at the sphere $\eta = 0$, the no-slip conditions give

$$v_r = v_\theta = 0, \quad \text{or} \quad f(0) = f'(0) = 0; \tag{26}$$

and since insignificant heating is supposed to have occurred, $T(0) = T_0$; whence from (5)

$$g(0) = \frac{T_0}{T_1} = \frac{(\gamma+1)^2}{2\gamma(\gamma-1)M_0^2}. \tag{27}$$

The remaining three conditions are found at the shock, $\eta = \eta_1$ say. From the shock relations (2) and (3), and using (22), we have

$$v_1 = -\frac{V_0(\gamma-1)}{(\gamma+1)} = -\frac{2}{a}Bf(\eta_1),$$

where $B = (V_0\nu_1 a)^{\frac{1}{2}}$: and substituting for $\nu_1$ this becomes

$$B = \left(\frac{4V_0^2a^2\gamma(\gamma-1)^2M_0^2}{(\gamma+1)^3R_0^2}\right)^{\frac{1}{2}},$$

where

$$R_0 = \frac{2V_0a\rho_0}{\mu_0} \quad \text{and} \quad M_0 = \frac{V_0}{c_0}$$

are the Reynolds number and Mach number. Hence we find

$$f(\eta_1) = \frac{1}{4}\left(\frac{R_0}{M_0^2}\frac{(\gamma+1)}{\gamma}\right)^{\frac{1}{2}}. \tag{28}$$

Also $$u_1 = V_0 = BCf'(\eta_1) = V_0f'(\eta_1),$$

whence $$f'(\eta_1) = 1; \tag{29}$$

and $T(\eta_1) = T_1$, whence $$g(\eta_1) = 1. \tag{30}$$

Using a simplified coding technique for a machine such as the Mercury electronic computer, the equations can be integrated from the sphere along an outward normal. Five boundary conditions at the sphere are needed to do this, and so two additional conditions on $f''(0)$ and $g'(0)$ are prescribed, approximate values being guessed from a crude polynomial solution.

As the problem stands, the shock-wave position is determined when $f'(\eta)$ and $g(\eta)$ are simultaneously equal to 1. It would therefore be necessary to try many runs with varying values of $f''(0)$, $g'(0)$ and $g(0)$ before this could be accomplished.

*Further transformations*

To get over the above difficulty, we first put

$$G = \frac{4(\gamma-1)}{(\gamma+1)^2}g, \tag{31}$$

so that (24) and (25) become

$$f''' + 2ff'' - f'^2 + G = 0, \tag{32}$$

and $$G'' + 2\sigma fG' = 0, \tag{33}$$

whereas the boundary conditions on $G$ are

$$G(0) = \frac{2}{\gamma M_0^2}, \tag{34}$$

$$G(\eta_1) = \frac{4(\gamma-1)}{(\gamma+1)^2}. \tag{35}$$

A shock-wave position is now determined when $f'(\eta_1) = 1$, and represents the solution for that value of $\gamma$ which satisfies (35). Unfortunately, $\gamma$, $M_0$ and $R_0$ are now determined uniquely by the boundary conditions (28), (34) and (35), and thus only one shock-wave flow is found for each set of initial conditions. This transformation then offers little improvement in the solution. Our final transformations, however, enable us to determine several flows for each integration.

First we choose a new variable

$$\alpha = \lambda\eta, \tag{36}$$

where $\lambda$ is a constant, and then by putting

$$f(\eta) = \lambda x(\alpha), \quad G(\eta) = \lambda^4 y(\alpha), \tag{37}$$

we are able to retain (32) and (33) in the same simple form:

$$x''' + 2xx'' - x'^2 + y = 0, \tag{38}$$

$$y'' + 2\sigma xy' = 0, \tag{39}$$

where the primes refer in this case to differentiation with respect to $\alpha$.

The boundary conditions, however, now include an arbitrary constant $\lambda$, and $\gamma$, $M_0$ and $R_0$ are not fixed by the boundary conditions, but depend on the value $\lambda$ takes.

We now have the conditions at $\alpha = 0$

$$x(0) = x'(0) = 0, \tag{40}$$

and

$$y(0) = \frac{2}{\gamma M_0^2 \lambda^4}. \tag{41}$$

At $\alpha = \alpha_1$, say, where $\alpha_1 = \lambda\eta_1$, we have

$$x(\alpha_1) = \left(\frac{R_0}{M_0^2}\frac{\gamma+1}{\gamma}\right)^{\frac{1}{2}} \Big/ 4\lambda, \tag{42}$$

$$x'(\alpha_1) = \frac{1}{\lambda^2}, \tag{43}$$

and

$$y(\alpha_1) = \frac{4(\gamma-1)}{(\gamma+1)^2\lambda^4}. \tag{44}$$

It should be noted that real solutions of (43) and (44) exist provided $x'(\alpha_1) > 0$ and $y(\alpha_1) \leqslant 0{\cdot}5$, and that the smaller of the two solutions of (44) for $\gamma$ is chosen on physical grounds.

The two most important advantages gained by these transformations are: (1) The boundary conditions can now be solved uniquely for $\gamma$, $M_0$ and $R_0$ at each integral step (subject to the above conditions). (2) There is no loss in generality

if we fix $y(0)$ and thus reduce the initial conditions to be varied from three to two. A convenient value useful in the polynomial solution is seen to be 0·02.

Another advantage is the added usefulness of the crude polynomial series method for finding suitable values of $x''(0)$ and $y'(0)$, since no longer does this type of solution have to apply to specific values of $\gamma$, $M_0$ and $R_0$. In fact it is only necessary to guarantee that $x'(\alpha)$ and $y(\alpha)$ increase steadily with $\alpha$ to assure satisfactory solutions of (43) and (44) and thus of (41) and (42) also.

## 3. Presentation of the results

*The tables*

The results obtained from the Mercury electronic computer by integrating equations (38) and (39) for 60 evenly spaced values of $x''(0)$ and $y'(0)$ were printed in the form of the tables 1 to 4, and others which are included in the author's thesis (Herring 1958).

| | 1 | 2 | 3 | 4 | 5 | 6 | 7 | 8 | 9 | 10 |
|---|---|---|---|---|---|---|---|---|---|---|
| | | $\int_0^\alpha y(\beta)\,d\beta$ | $x(\alpha)y(\alpha)$ | $x'(\alpha)$ | $x''(\alpha)/y(\alpha)$ | $y(\alpha)$ | $y'(\alpha)/y(\alpha)$ | | | |
| | $\alpha = 0$ | 0·000 | 0·000 | 0·000 | 30·000 | 0·020 | 12·500 | | | |
| | $\alpha = 0{\cdot}2$ | 0·009 | 0·001 | 0·119 | 8·445 | 0·070 | 3·568 | | | |
| | $\alpha = 0{\cdot}6$ | 0·057 | 0·018 | 0·347 | 3·221 | 0·169 | 1·436 | | | |
| | $\alpha = 1{\cdot}0$ | 0·143 | 0·075 | 0·550 | 1·776 | 0·262 | 0·831 | | | |
| | | 0·264 | 0·184 | 0·717 | 1·093 | 0·340 | 0·505 | | | |
| | | 0·412 | 0·340 | 0·849 | 0·730 | 0·397 | 0·290 | | | |
| | | 0·579 | 0·527 | 0·953 | 0·545 | 0·433 | 0·147 | | | |
| | $\frac{b-a}{a}$ | 0·756 | 0·728 | 1·041 | 0·464 | 0·451 | 0·063 | | | |
| | | 0·937 | 0·938 | 1·122 | 0·435 | 0·458 | 0·021 | $\gamma$ | $M_0$ | $R_0$ |
| 1 | 0·1158 | 1·121 | 1·156 | 1·201 | 0·427 | 0·460 | 0·006 | 1·497 | 9·82 | 4,860 |
| *2 | 0·1020 | 1·305 | 1·386 | 1·280 | 0·425 | 0·460 | 0·001 | 1·407 | 10·79 | 7,700 |
| 3 | 0·0908 | 1·489 | 1·629 | 1·358 | 0·425 | 0·461 | 0·000 | 1·343 | 11·72 | 11,600 |
| *4 | 0·0816 | 1·673 | 1·886 | 1·436 | 0·425 | 0·461 | 0·000 | 1·294 | 12·63 | 16,810 |
| 5 | 0·0738 | 1·858 | 2·158 | 1·514 | 0·425 | 0·461 | 0·000 | 1·255 | 13·52 | 23,590 |
| 6 | 0·0672 | 2·042 | 2·444 | 1·593 | 0·425 | 0·461 | 0·000 | 1·225 | 14·39 | 32,260 |
| *7 | 0·0615 | 2·226 | 2·745 | 1·671 | 0·425 | 0·461 | 0·000 | 1·200 | 15·25 | 43,170 |

TABLE 1. The shock data used in figures 2 and 6 are indicated by *. Rows in this table only are printed at intervals of $\alpha = 0{\cdot}4$ except for the first step.

In each table the columns are numbered from 1 to 10. The columns 2–7 are functions of $\alpha$, chosen to be directly proportional to the velocity and temperature variables, and columns 1, 8, 9 and 10 give the shock stand-off distances and the values of $\gamma$, $M_0$ and $R_0$. The rows are printed at intervals of $\alpha = 0{\cdot}2$ except in table 1 where intervals of $\alpha = 0{\cdot}4$ are used for brevity, and those numbered represent the positions of the shock waves. It must be remembered that each table gives a picture of the flow across several completely independent boundary layers. This is clear from the relationships connecting the columns, which are functions of $\alpha$, with those expressed in terms of $r$. The constants connecting them, which are different for each shock, are inserted in square brackets, in the following expressions.

Column 1 gives the ratio of the stand-off distances of the shocks to the sphere radius, namely

$$\frac{b-a}{a} = \frac{\gamma+1}{8x(\alpha_1)\,x'(\alpha_1)} \int_0^{\alpha_1} y(\beta)\,d\beta, \tag{45}$$

| | 1 | 2 | 3 | 4 | 5 | 6 | 7 | 8 | 9 | 10 |
|---|---|---|---|---|---|---|---|---|---|---|
| | | $\int_0^\alpha y(\beta)\,d\beta$ | $x(\alpha)y(\alpha)$ | $x'(\alpha)$ | $x''(\alpha)/y(\alpha)$ | $y(\alpha)$ | $y'(\alpha)/y(\alpha)$ | | | |
| | | 0·000 | 0·000 | 0·000 | 40·000 | 0·020 | 12·500 | | | |
| | | 0·009 | 0·001 | 0·159 | 11·303 | 0·070 | 3·567 | | | |
| | | 0·028 | 0·008 | 0·316 | 6·451 | 0·120 | 2·063 | | | |
| | | 0·057 | 0·024 | 0·468 | 4·417 | 0·168 | 1·424 | | | |
| | | 0·095 | 0·054 | 0·613 | 3·291 | 0·215 | 1·054 | | | |
| | | 0·143 | 0·100 | 0·751 | 2·580 | 0·259 | 0·801 | | | |
| | $\frac{b-a}{a}$ | 0·198 | 0·164 | 0·880 | 2·099 | 0·298 | 0·609 | | | |
| | | 0·261 | 0·244 | 1·001 | 1·766 | 0·331 | 0·455 | $\gamma$ | $M_0$ | $R_0$ |
| *1 | 0·0945 | 0·330 | 0·340 | 1·114 | 1·535 | 0·358 | 0·330 | 1·423 | 9·34 | 660 |
| 2 | 0·0821 | 0·404 | 0·448 | 1·221 | 1·377 | 0·378 | 0·230 | 1·351 | 10·50 | 1,160 |
| *3 | 0·0725 | 0·481 | 0·565 | 1·323 | 1·275 | 0·393 | 0·152 | 1·296 | 11·62 | 1,900 |
| 4 | 0·0648 | 0·560 | 0·689 | 1·421 | 1·211 | 0·403 | 0·094 | 1·253 | 12·70 | 2,960 |
| 5 | 0·0584 | 0·641 | 0·819 | 1·518 | 1·175 | 0·408 | 0·054 | 1·218 | 13·76 | 4,410 |
| *6 | 0·0529 | 0·723 | 0·955 | 1·614 | 1·155 | 0·412 | 0·029 | 1·190 | 14·79 | 6,340 |
| 7 | 0·0482 | 0·806 | 1·096 | 1·709 | 1·146 | 0·413 | 0·014 | 1·166 | 15·82 | 8,870 |

TABLE 2. The shock data used in figures 3 and 7 are indicated by *.

| | 1 | 2 | 3 | 4 | 5 | 6 | 7 | 8 | 9 | 10 |
|---|---|---|---|---|---|---|---|---|---|---|
| | | $\int_0^\alpha y(\beta)\,d\beta$ | $x(\alpha)y(\alpha)$ | $x'(\alpha)$ | $x''(\alpha)/y(\alpha)$ | $y(\alpha)$ | $y'(\alpha)/y(\alpha)$ | | | |
| | | 0·000 | 0·000 | 0·000 | 60·000 | 0·200 | 32·500 | | | |
| | | 0·017 | 0·004 | 0·239 | 7·891 | 0·150 | 4·326 | | | |
| | | 0·060 | 0·027 | 0·472 | 4·091 | 0·279 | 2·289 | | | |
| | | 0·128 | 0·086 | 0·693 | 2·660 | 0·404 | 1·513 | | | |
| | | 0·221 | 0·194 | 0·900 | 1·900 | 0·522 | 1·078 | | | |
| | | 0·336 | 0·358 | 1·089 | 1·433 | 0·628 | 0·783 | | | |
| | | 0·470 | 0·578 | 1·260 | 1·127 | 0·717 | 0·563 | | | |
| | $\frac{b-a}{a}$ | 0·621 | 0·847 | 1·413 | 0·925 | 0·789 | 0·391 | | | |
| | | 0·784 | 1·152 | 1·553 | 0·794 | 0·841 | 0·258 | $\gamma$ | $M_0$ | $R_0$ |
| 1 | 0·1037 | 0·955 | 1·484 | 1·682 | 0·714 | 0·876 | 0·159 | 1·474 | 13·85 | 3,120 |
| *2 | 0·0921 | 1·133 | 1·834 | 1·804 | 0·668 | 0·898 | 0·091 | 1·396 | 15·27 | 5,030 |
| 3 | 0·0826 | 1·314 | 2·198 | 1·922 | 0·644 | 0·910 | 0·047 | 1·336 | 16·63 | 7,680 |
| *4 | 0·0747 | 1·496 | 2·576 | 2·039 | 0·633 | 0·916 | 0·022 | 1·289 | 17·96 | 11,270 |
| 5 | 0·0679 | 1·680 | 2·969 | 2·154 | 0·628 | 0·919 | 0·009 | 1·251 | 19·26 | 15,990 |
| *6 | 0·0620 | 1·864 | 3·380 | 2·270 | 0·627 | 0·920 | 0·004 | 1·220 | 20·55 | 22,070 |

TABLE 3. The shock data used in figures 4 and 8 are indicated by *.

| | 1 | 2 | 3 | 4 | 5 | 6 | 7 | 8 | 9 | 10 |
|---|---|---|---|---|---|---|---|---|---|---|
| | | $\int_0^\alpha y(\beta)\,d\beta$ | $x(\alpha)y(\alpha)$ | $x'(\alpha)$ | $x''(\alpha)/y(\alpha)$ | $y(\alpha)$ | $y'(\alpha)/y(\alpha)$ | | | |
| | | 0·000 | 0·000 | 0·000 | 70·000 | 0·020 | 32·500 | | | |
| | | 0·017 | 0·004 | 0·279 | 9·226 | 0·150 | 4·324 | | | |
| | | 0·060 | 0·031 | 0·552 | 4·812 | 0·279 | 2·284 | | | |
| | | 0·128 | 0·100 | 0·813 | 3·164 | 0·403 | 1·501 | | | |
| | $\frac{b-a}{a}$ | 0·220 | 0·226 | 1·061 | 2·301 | 0·519 | 1·058 | | | |
| | | 0·334 | 0·417 | 1·291 | 1·781 | 0·621 | 0·755 | $\gamma$ | $M_0$ | $R_0$ |
| 1 | 0·1013 | 0·467 | 0·670 | 1·503 | 1·450 | 0·705 | 0·527 | 1·480 | 12·36 | 880 |
| *2 | 0·0844 | 0·614 | 0·978 | 1·700 | 1·239 | 0·769 | 0·351 | 1·375 | 14·50 | 1,850 |
| *3 | 0·0724 | 0·773 | 1·327 | 1·886 | 1·110 | 0·814 | 0·219 | 1·304 | 16·51 | 3,480 |
| 4 | 0·0632 | 0·938 | 1·705 | 2·063 | 1·036 | 0·842 | 0·125 | 1·251 | 18·45 | 6,010 |
| *5 | 0·0558 | 1·108 | 2·105 | 2·235 | 0·997 | 0·857 | 0·065 | 1·209 | 20·32 | 9,750 |

TABLE 4. The shock data used in figures 5 and 9 are indicated by *.

whereas column 2 gives

$$\int_0^{\alpha} y(\beta)\,d\beta.$$

This can be converted to $(r-a)/a$ upon multiplying by $[(\gamma+1)/8x(\alpha_1)\,x'(\alpha_1)]$, but this is more quickly found from (45) as $\left[(b/a-1)\Big/\int_0^{\alpha_1} y(\beta)\,d\beta\right]$ by dividing the corresponding values in columns 1 and 2. Note that the suffix 1 denotes the values immediately behind the shock and these are given in numbered rows.

The next five columns, 3–7, are connected to the velocities and temperature as follows. Column 3 gives $x(\alpha)\,y(\alpha)$, where the ratio of the radial component of the velocity behind the shock to that ahead is $-v(r)\cos\theta/V_0\cos\theta$, where

$$\frac{v(r)}{V_0} = \left[-\left(\frac{\gamma-1}{\gamma+1}\right)\Big/x(\alpha_1)\,y(\alpha_1)\right]x(\alpha)\,y(\alpha). \tag{46}$$

The transverse component is quickly found from column 4, which gives $x'(\alpha)$, since

$$\frac{u(r)}{V_0} = \left[\frac{1}{x'(\alpha_1)}\right]x'(\alpha). \tag{47}$$

To obtain $[du(r)/dr]/V_0/a$, column 5 must be multiplied by $[8x(\alpha_1)/(\gamma+1)]$. The temperature ratio is

$$\frac{T(r)}{T_0} = \frac{y(\alpha)}{y(0)} = [50]\,y(\alpha), \tag{48}$$

where $y(\alpha)$ is given in column 6, and finally column 7 gives $y'(\alpha)/y(\alpha)$, where the constant needed to give $[dT(r)/dr]/[T_0/a]$ is

$$\left[\frac{8}{\gamma+1}\frac{x(\alpha_1)\,x'(\alpha_1)}{y(0)}\right] = \left[\frac{400}{\gamma+1}\,x(\alpha_1)\,x'(\alpha_1)\right]. \tag{49}$$

Certain information can be found by direct reading of the tables. For instance, the edges of the velocity and temperature boundary layers are approached when columns 5, 6 and 7, which are related to $du/dr$, $T$ and $dT/dr$, tend to a constant value. This is very clearly seen in, for example, table 1 (see also figure 2), and in this, as in a few other cases, the shocks are well outside the boundary-layer section. The assumption of a constant pressure throughout the region behind the shock (12) will be less accurate in these cases.

In the table mentioned above the thickness of the velocity and temperature boundary layers are seen to be of the same order, and this is due to the nearness of the Prandtl number (0·72) to unity.

### *The graphs*

Three temperature and two transverse velocity profiles have been drawn for tables 1–4. Figures 2–5 give the temperature and figures 6–9 the velocity profiles for each of these tables, taken in order. The magnitude of the temperatures reached depends directly on the shock relations and a comparison of figures 2 and 4 gives some idea of the range considered.

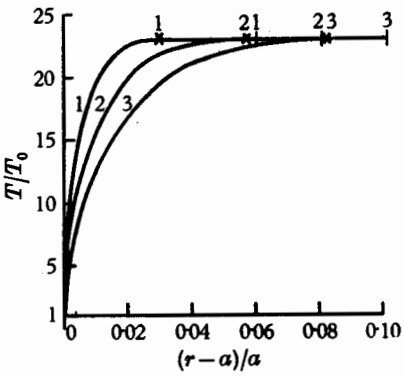


FIGURE 2

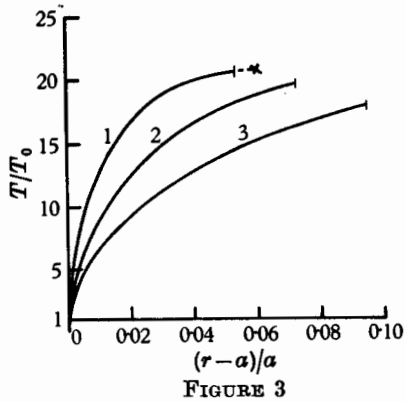


FIGURE 3

FIGURE 2. Temperature profiles plotted from data given in table 1. N.B. In figures 2–9 a shock wave is denoted by a stroke | and approximate boundary-layer edges by a cross ×; the number above is the curve number. Curve 1: $\gamma = 1{\cdot}200$, $M_0 = 15{\cdot}25$, $R_0 = 43{,}170$. Curve 2: $\gamma = 1{\cdot}294$, $M_0 = 12{\cdot}63$, $R_0 = 16{,}810$. Curve 3: $\gamma = 1{\cdot}407$, $M_0 = 10{\cdot}79$, $R_0 = 7700$.

FIGURE 3. Temperature profiles plotted from data given in table 2. In curves 1 of figures 3–5 the shock-wave positions and the boundary-layer edges suggested by the profiles have been marked. In actual fact of course, the boundary layer will end at the shock wave, since ahead of it the temperature assumes the constant value $T_0$, and so outside the shock the curve is shown as a dotted line. Curve 1: $\gamma = 1{\cdot}190$, $M_0 = 14{\cdot}79$, $R_0 = 6340$. Curve 2: $\gamma = 1{\cdot}296$, $M_0 = 11{\cdot}62$, $R_0 = 1900$. Curve 3: $\gamma = 1{\cdot}423$, $M_0 = 9{\cdot}34$, $R_0 = 660$.

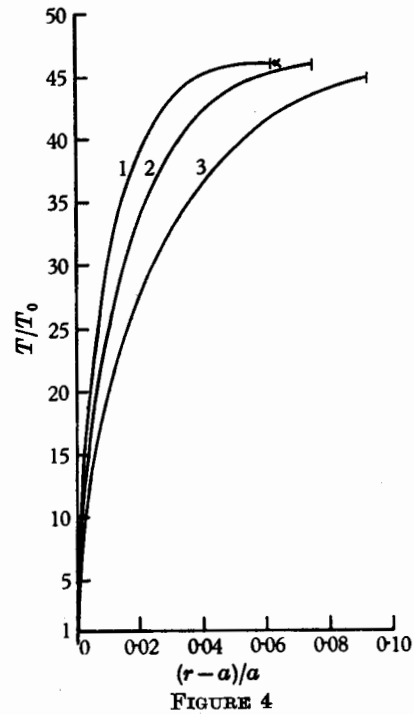


FIGURE 4

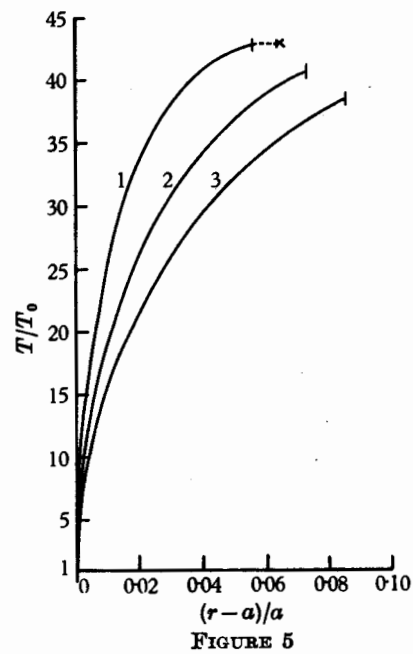


FIGURE 5

FIGURE 4. Temperature profiles plotted from data given in table 3. Curve 1: $\gamma = 1{\cdot}220$, $M_0 = 20{\cdot}55$, $R_0 = 22{,}070$. Curve 2: $\gamma = 1{\cdot}289$, $M_0 = 17{\cdot}96$, $R_0 = 11{,}270$. Curve 3: $\gamma = 1{\cdot}396$, $M_0 = 15{\cdot}27$, $R_0 = 5030$.

FIGURE 5. Temperature profiles plotted from data given in table 4. Curve 1: $\gamma = 1{\cdot}209$, $M_0 = 20{\cdot}32$, $R_0 = 9750$. Curve 2: $\gamma = 1{\cdot}304$, $M_0 = 16{\cdot}51$, $R_0 = 3480$. Curve 3: $\gamma = 1{\cdot}375$, $M_0 = 14{\cdot}50$, $R_0 = 1850$.

Naturally in this problem we are most interested in, for example, the shock stand-off distance, or the boundary-layer thickness as a function of the Reynolds number $R_0$ or Mach number $M_0$. To find the variation with $R_0$, we must maintain $\gamma$ and $M_0$ at constant values.

A comparison of curves 1 in figures 2 and 3 and also curves 1 in figures 4 and 5, where in each pair $\gamma$ and $M_0$ are approximately constant, gives an indication of this behaviour. The approximate boundary-layer edges have been marked on these graphs with a cross and in these examples as $R_0$ increases the gradients get larger and thus the boundary-layer thickness decreases. However, at the same time it is surprising that the shock stand-off distance (marked with a dash) increases with $R_0$. This last result is borne out in a more detailed investigation later.

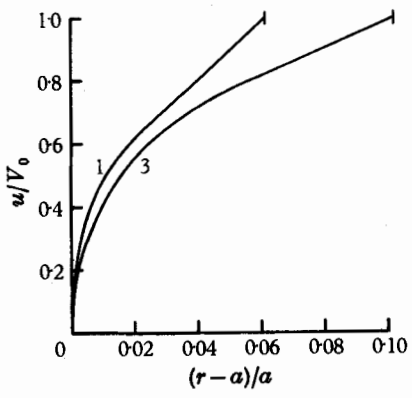


FIGURE 6

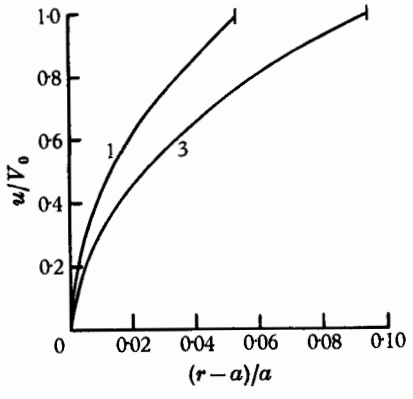


FIGURE 7

FIGURE 6. Transverse velocity profile plotted from data given in table 1. Curve 1: $\gamma = 1{\cdot}200$, $M_0 = 15{\cdot}25$, $R_0 = 43{,}170$. Curve 3: $\gamma = 1{\cdot}407$, $M_0 = 10{\cdot}79$, $R_0 = 7700$.

FIGURE 7. Transverse velocity profile plotted from data given in table 2. Curve 1: $\gamma = 1{\cdot}190$, $M_0 = 14{\cdot}79$, $R_0 = 6340$. Curve 2: $\gamma = 1{\cdot}423$, $M_0 = 9{\cdot}34$, $R_0 = 660$.

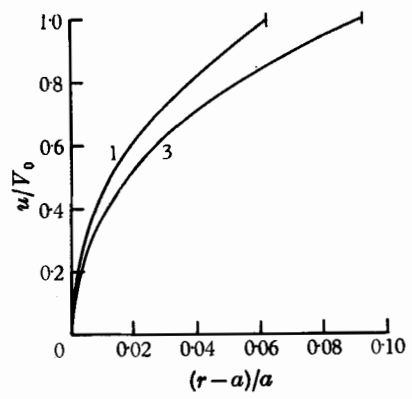


FIGURE 8

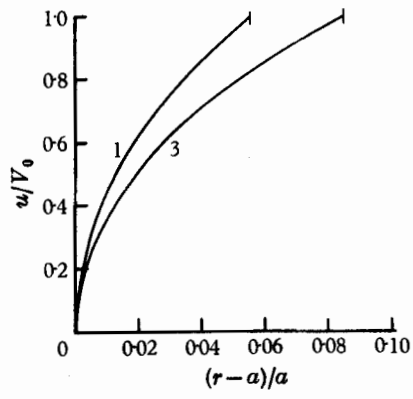


FIGURE 9

FIGURE 8. Transverse velocity profile plotted from data given in table 3. Curve 1: $\gamma = 1{\cdot}220$, $M_0 = 20{\cdot}55$, $R_0 = 22{,}070$. Curve 3: $\gamma = 1{\cdot}396$, $M_0 = 15{\cdot}27$, $R_0 = 5030$.

FIGURE 9. Transverse velocity profile plotted from data given in table 4. Curve 1: $\gamma = 1{\cdot}209$, $M_0 = 20{\cdot}32$, $R_0 = 9750$. Curve 3: $\gamma = 1{\cdot}375$, $M_0 = 14{\cdot}50$, $R_0 = 1850$.

In figures 6–9 showing the transverse velocity profiles, the edge of the boundary layer is defined by a region of approximately constant shear flow. In other words, in a region where viscosity has little effect the vorticity shed by a shock wave of constant curvature is constant. The outer parts of these graphs agree quite well with the exact inviscid incompressible solutions obtained by Lighthill (1957) for a gas with varying specific heats. The effect of viscosity in reducing the velocity quickly to zero is very marked.

The remaining graphs, figures 10–16, show the variation of certain quantities at constant values of $\gamma$ and $M_0$, and provide a very interesting insight into their behaviour in a hypersonic flow.

Interpolation on a large scale is an unfortunate necessity in this method, where $\gamma$, $M_0$ and $R_0$ are not predetermined, and to maintain $\gamma$ and $M_0$ constant, a three-point linear scheme between two tables was used.

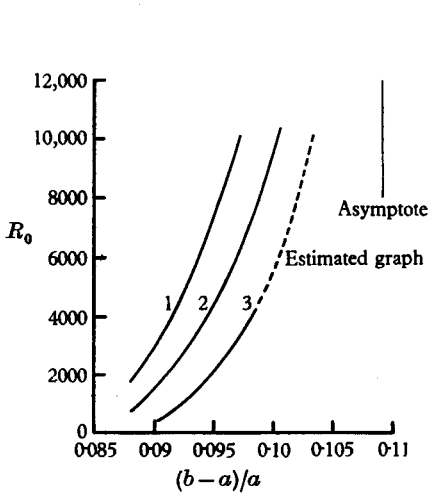


FIGURE 10

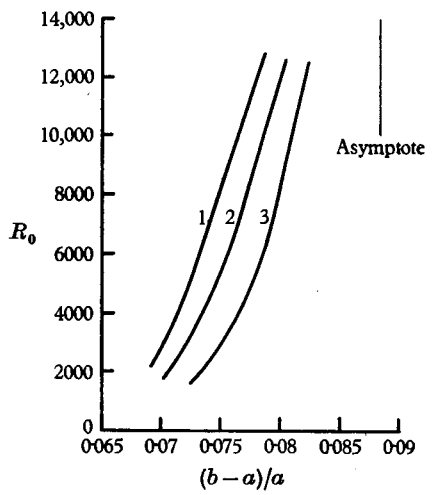


FIGURE 11

FIGURE 10. The Reynolds number as a function of the ratio stand-off distance of the shock to sphere radius, when $\gamma = 1{\cdot}4$. Curve 1: $M_0 = 15$. Curve 2: $M_0 = 12$. Curve 3: $M_0 = 9$.
FIGURE 11. The Reynolds number as a function of the ratio stand-off distance of shock to sphere radius, when $\gamma = 1{\cdot}3$. Curve 1: $M_0 = 18$. Curve 2: $M_0 = 15$. Curve 3: $M_0 = 12$.

Figures 10–12 show the variation of $R_0$ with the ratio of stand-off distance to sphere radius for a number of constant values of $\gamma$ and $M_0$. The interesting result, hinted at previously, that the shock stand-off distance increases with Reynolds number, is here verified, and the asymptotes to the graph (which are independent of Mach number) are drawn for each value of $\gamma$. Can this mean that we have negative displacement thicknesses? A comparison of figure 2 with 3, and figure 4 with 5 gives an indication that the boundary-layer thickness decreases with increase in Reynolds number and an examination of the product $\rho u$ in these cases shows that it decreases from a maximum at the shock to a minimum at the sphere. In other words, the displacement thickness given by $\int_a^b (u_1\rho_1 - u(r)\rho(r))\,dr$ is positive. The shock distance, however, is not governed by the boundary-layer

thickness, for in table 1 the shocks are outside, and in tables 2–4 they are inside the boundary layer, and thus it is probable that this idea of displacement thickness is erroneous for the region behind the shock. If the shock position depended more upon distribution of mass than of mass flow, i.e. depended more upon $\rho$ and $\rho u$, then a 'mass defect' given by $\int_a^b (\rho_1 - \rho(r))\,dr$ would certainly be negative, and the shock distance would increase with increase in the Reynolds number.

A rough interpolation within figures 10–12 to maintain constant $\gamma$, and between them to maintain constant $M_0$, shows that the shock distance decreases with increase in Mach number and with decrease in $\gamma$, respectively. A simple analysis of the boundary conditions on the density at the shock and the sphere, and the knowledge that the density decreases continuously outwards from the sphere

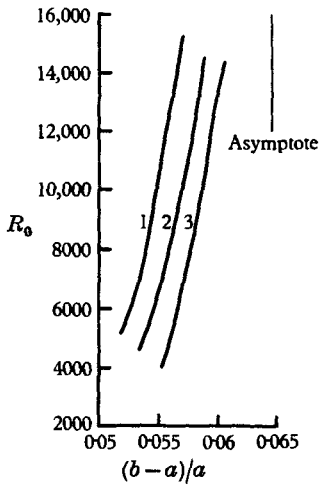


FIGURE 12. The Reynolds number as a function of the ratio stand-off of shock to sphere radius, when $\gamma = 1{\cdot}2$. Curve 1: $M_0 = 18$. Curve 2: $M_0 = 15$. Curve 3: $M_0 = 12$.

provides a simple explanation of these results. The strong shock condition on the density (2) is independent of Mach number, whilst the density at the sphere, which, since $T(0) = T_0$, is dependent only upon the pressure given by (4), increases with Mach number. The region therefore is further compressed and the shock wave moves closer to the body as the Mach number increases. A similar consideration of (2) and (4) shows that as $\gamma$ increases, the density just behind the shock decreases, whilst at the sphere it remains effectively constant. The shock in this case, therefore, moves away from the sphere as $\gamma$ increases.

A note here about the error caused by assuming the strong shock conditions on the density will be of value. The oblique shock relation for the density is

$$\frac{\rho_1}{\rho_0} = \left(\frac{\gamma+1}{\gamma-1}\right) \frac{1}{(1+2/(\gamma-1)\,M_0^2)}, \tag{50}$$

where terms $O(\theta^2)$ have been neglected. The strong shock relations are only valid if $\frac{1}{2}M_0^2(\gamma-1) \gg 1$ which means, for example when $\gamma = 1{\cdot}4$, that $M_0^2$ must be much greater than 5 for these relations to be used. The lowest Mach number considered

at $\gamma = 1{\cdot}4$ is 9, and substituting in (50) gives $\rho_1/\rho_0 \doteq 0{\cdot}94(\gamma+1)/(\gamma-1)$. It is clear from this that the strong shock conditions tend to overestimate the density, and so the correction to the graphs involves a small shift to the right to give a compensating increase in the shock stand-off distance. This correction will of course decrease as the Mach number increases.

Figures 13 and 14, where the ratio of $(r-a)$ at $T = 0{\cdot}98T_1$ to $(r-a)$ at $T = T_1$, i.e. $(b-a)$, is plotted against $\log_{10}R_0$, give an indication of the variation of the boundary-layer thickness with Reynolds number. The decrease in the ratio with increase in $R_0$ shows clearly that the temperature gradients are increasing, and this supports the idea that the boundary-layer width is decreasing with increase

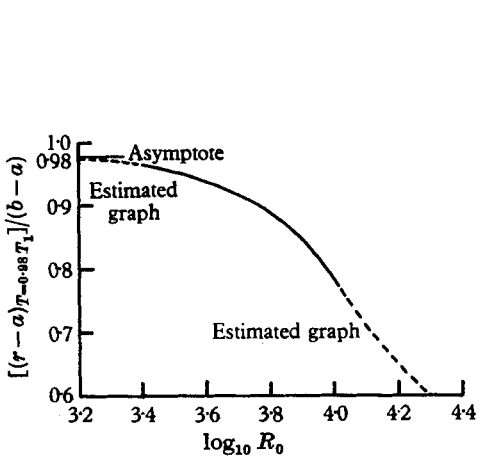


FIGURE 13

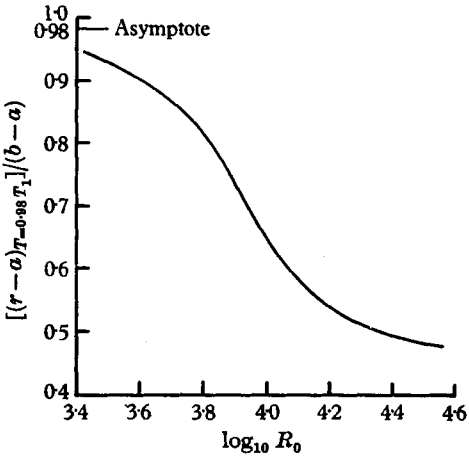


FIGURE 14

FIGURE 13. Boundary-layer thickness as a function of shock stand-off distance, as indicated by the ratio $[(r-a)_{T=0\cdot98T_1}]/(b-a)$, for $\gamma = 1{\cdot}3$ and $M_0 = 18$.

FIGURE 14. Boundary-layer thickness as a function of the shock stand-off distance as indicated by the ratio $[(r-a)_{T=0\cdot98T_1}]/(b-a)$, for $\gamma = 1{\cdot}2$ and $M_0 = 15$.

in $R_0$. At low Reynolds number, where the profile approximates to a straight line, the ratio approaches 0·98, and it decreases through a point of inflexion before tending to a further constant value for large values of $R_0$.

Finally figures 15 and 16 show the variation of skin friction with the Reynolds number, where the skin-friction coefficient is defined as

$$c_f = \frac{\mu_0[du(r)/dr]_{r=a}}{\frac{1}{2}\rho_0 V_0^2} = \frac{400x''(0)}{[\gamma(\gamma+1)]^{\frac{1}{4}}M_0},$$

and it is noticeable that, with $\gamma$ and $M_0$ held constant, $c_f$ is solely dependent upon the initial value of $x''(\alpha)$. Once more the influence of the shock wave on the flow can be clearly seen, for, instead of $c_f R_0^{\frac{1}{2}}$ having a constant value as suggested by boundary-layer theory, it is seen to decrease with increase in $R_0$. In fact, when $R_0$ is of order $10^3$, $c_f$ behaves more like $R_0^{-1}$. However, the graphs seem to indicate that $c_f R_0^{\frac{1}{2}}$ does approach a constant value at higher Reynolds numbers, and this is not surprising since the tabulated results indicate that when $R_0$ is of order $10^4$ the

shock waves lie well outside the boundary layer, and thus one would expect the normal boundary approximations to apply.

The approximate solutions which have been found for the problem have only been explained in part, but further clarification should be possible as more becomes known about flows at very high speeds.

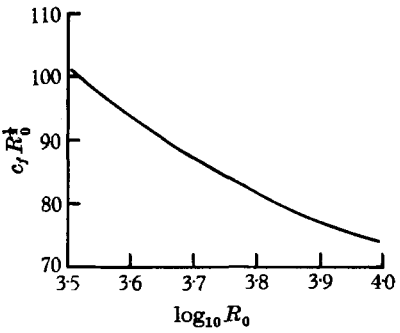


FIGURE 15

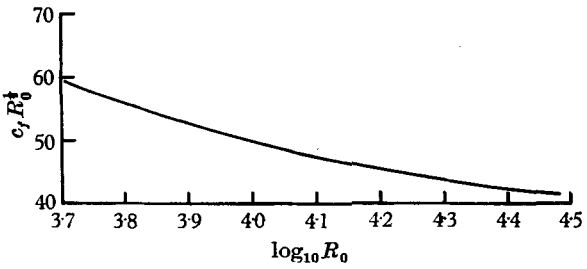


FIGURE 16

FIGURE 15. The skin-friction coefficient as a function of the Reynolds number, for $\gamma = 1{\cdot}3$ and $M_0 = 18$.

FIGURE 16. The skin-friction coefficient as a function of the Reynolds number, for $\gamma = 1{\cdot}2$ and $M_0 = 15$.

I would like to thank Prof. M. J. Lighthill and Mr C. R. Illingworth for their help and encouragement at all times, and also Mr R. Kerr for his advice on programming for the Mercury computer.

## REFERENCES

BROWN, W. B. & DONOUGHE, P. L. 1951 *Nat. Adv. Comm. Aero. Tech., Wash., Note* 2479.
CHESTER, W. 1956 *J. Fluid Mech.* **1**, 353, 490.
FREEMAN, N. C. 1956 *J. Fluid Mech.* **1**, 366.
HERRING, T. K. 1958 M.Sc. Thesis, Manchester University.
HOMANN, F. 1936 *Z. Angew. Math. Mech.* **16**, 153.
LIGHTHILL, M. J. 1957 *J. Fluid Mech.* **2**, 1.
OLIVER, R. E. 1956 *J. Aero. Sci.* **23**, 177.
WHIPPLE, F. L. 1943 *Rev. Mod. Phys.* **15**, 246.